Atmos. Chem. Phys., 23, 2365–2378, 2023
https://doi.org/10.5194/acp-23-2365-2023

Atmospheric Chemistry and Physics
Open Access
EGU

Research article

The shifting of secondary inorganic aerosol formation mechanisms during haze aggravation: the decisive role of aerosol liquid water

Fei Xie[1,2], Yue Su[1,3], Yongli Tian[2], Yanju Shi[2], Xingjun Zhou[2], Peng Wang[2], Ruihong Yu[1], Wei Wang[1], Jiang He[1,3], Jinyuan Xin[4], and Changwei Lü[1,3]

[1]School of Ecology and Environment, Inner Mongolia University, 010021, Hohhot, China
[2]Inner Mongolia Environmental Monitoring Center, 010011, Hohhot, China
[3]Institute of Environmental Geology, Inner Mongolia University, 010021, Hohhot, China
[4]State Key Laboratory of Atmospheric Boundary Layer Physics and Atmospheric Chemistry (LAPC), Institute of Atmospheric Physics, Chinese Academy of Sciences, Beijing, 100029, China

Correspondence: Jinyuan Xin (xjy@mail.iap.ac.cn) and Changwei Lü (lcw2008@imu.edu.cn)

Received: 18 August 2022 – Discussion started: 10 October 2022
Revised: 16 January 2023 – Accepted: 2 February 2023 – Published: 21 February 2023

Abstract. Although many considerable efforts have been done to reveal the driving factors on haze aggravation, however, the roles of aerosol liquid water (ALW) in secondary inorganic aerosol (SIA) formation were mainly focused on the condition of aerosol liquid water content (ALWC) $< 100\,\mu g\,m^{-3}$. Based on the in situ high-resolution field observations, this work studied the decisive roles and the shifting of secondary inorganic aerosol formation mechanisms during haze aggravation, revealing the different roles of ALWC on a broader scale ($\sim 500\,\mu g\,m^{-3}$) in nitrate and sulfate formation induced by aqueous chemistry in the ammonia-rich atmosphere. The results showed that chemical domains of perturbation gas limiting the generation of secondary particulate matter presented obvious shifts from a HNO_3-sensitive to a HNO_3- and NH_3-co-sensitive regime with the haze aggravation, indicating the powerful driving effects of ammonia in the ammonia-rich atmosphere. When ALWC $< 75\,\mu g\,m^{-3}$, the sulfate generation was preferentially triggered by the high ammonia utilization and then accelerated by nitrogen oxide oxidation from clean to moderate pollution stages, characterized by nitrogen oxidation ratio (NOR) < 0.3, sulfur oxidation ratio (SOR) < 0.4, ammonia transition ratio (NTR) < 0.7 and the moral ratio of $NO_3^-/SO_4^{2-} = 2:1$. When ALWC $> 75\,\mu g\,m^{-3}$, the aqueous-phase chemistry reaction of SO_2 and NH_3 in ALW became the prerequisite for SIA formation driven by Henry's law in the ammonia-rich atmosphere during heavy and serious stages, characterized by high SOR (0.5–0.9), NOR (0.3–0.5) and NTR (> 0.7), as well as the high moral ratio of $NO_3^-/SO_4^{2-} = 1:1$. A positive feedback of sulfate on nitrate production was also observed in this work due to the shift in ammonia partitioning induced by the ALWC variation during haze aggravation. It implies the target controlling of haze should not simply focus on SO_2 and NO_2, but more attention should be paid to gaseous precursors (e.g., SO_2, NO_2, NH_3) and aerosol chemical constitution during different haze stages.

Published by Copernicus Publications on behalf of the European Geosciences Union.

1 Introduction

Fine particulate matter ($PM_{2.5}$) presented a close link with several environmental issues, such as visibility reduction and climate change (Zhang et al., 2015; Shang et al., 2020; Wang et al., 2016, 2020; Nozière et al., 2010). Epidemiological studies have stated the association of PM with public health and even adverse birth outcomes (Gwynn et al., 2000; Lavigne et al., 2016; Zhao et al., 2020). As the most abundant secondary inorganic aerosols (SIAs) in $PM_{2.5}$ during Chinese winter haze episodes (Fu and Chen, 2017; Liu et al., 2019), the formation of sulfate and nitrate plays a key role during haze aggravation, as well as having an impact on the oxidants in gas and aqueous phases; the characteristics of pre-existing aerosols, fog and cloud; and meteorological conditions. Recently, aerosol liquid water content (ALWC) was reported as being associated with SIA formation, especially sulfates and nitrates, during the haze periods (Wu et al., 2018; B. Zheng et al., 2015; Wang et al., 2016; Cheng et al., 2016; Carlton and Turpin, 2013; Nguyen et al., 2014; Xue et al., 2014; Tan et al., 2017; Z. Liu et al., 2017). Atmospheric aerosol liquid water (ALW), which is determined by ambient relative humidity (RH), has been proposed as a container since it could provide the reaction medium for the multiphase chemistry during the haze process (Ansari and Pandis, 2000; Shiraiwa et al., 2012; Davies and Wilson, 2015). The roles of ALWC on the generation of particulate sulfate (Wang et al., 2016; Cheng et al., 2016) and global secondary organic aerosols (Hodas et al., 2014; McNeill, 2015; Wong et al., 2015) were reported. Thus, fully understanding ALW and its roles during haze aggravation is fundamentally important for atmospheric physicochemical processes, especially the liquid chemical transformation of SO_2 and NO_x in ALW.

Ammonia is the most important alkaline gas, neutralizing with acidic species to form ammonium salts. Due to little attention having been paid to NH_3 emissions by the Chinese government, atmospheric NH_3 experienced a significant increasing trend (Ge et al., 2019; Tan et al., 2017). Although the increase in atmospheric NH_3 is beneficial to reduce atmospheric acidity (Liu et al., 2019), its chemical behavior in regional haze formation is still being debated. Cheng et al. (2016) indicated that the fast transform of gaseous SO_2 to particle sulfate under polluted conditions is attributed to the neutralization of NH_3, which raises particle pH and thereby facilitated the aqueous oxidation of S(VI) by NO_2. Fang et al. (2017) stated that NH_3 partitioning significantly modified aerosol pH and thereby adjusted the partitioning of SO_2 and NO_2. Although the role of NH_3 has been identified from a theoretical perspective, the lack of NH_3 emission control sets barriers for a more effective reduction of $PM_{2.5}$. Therefore, it is urgent to fully understand the reactive gases' behavior and the chemical mechanisms of SIA formation during different pollution stages, which will be helpful in proposing reasonable strategies for each stage.

So far, the SIA formation has been extensively studied during short-term, continuous or persistent haze episodes, and several heterogeneous and homogeneous oxidation pathways for sulfate and nitrate formation have been proposed (Guo et al., 2014, 2017; G. J. Zheng et al., 2015; Huang et al., 2014; Liu et al., 2019, 2021; Yao et al., 2020; Zhou et al., 2018). In the ammonia-rich atmosphere, NH_3 partitioning significantly modified aerosol pH, adjusted the partitioning of SO_2 and NO_2 (Fang et al., 2017), and promoted the aqueous oxidation of S(VI) by NO_2 (Wang et al., 2016; Cheng et al., 2016). Although many considerable efforts have been done to reveal the driving factors of haze aggravation, however, the roles of ALW in SIA formation were mainly focused on the condition of ALWC $< 100\,\mu g\,m^{-3}$ (Nenes et al., 2020; Wu et al., 2018; Bian et al., 2014; Jin et al., 2020). Therefore, the roles of ALWC on a broader scale and the shifting mechanisms of secondary inorganic aerosol formation during haze aggravation in the ammonia-rich atmosphere need to be understood in depth. Based on a continuous observations with 1 h resolution from December 2019 to January 2020, this work discusses the shift in the dominant mechanisms with ALWC variation during the time window of haze aggravation processes, which will be helpful in proposing more effective $PM_{2.5}$ control strategies for each pollution stage.

2 Sampling and experiment methods

2.1 Description of sampling site

Hohhot, the capital city of the Inner Mongolia Autonomous Region, is the central city of the Hohhot–Baotou–Ordos group, as well as an important northern Chinese city with a population of more than 3.126 million and an area of $17\,224\,km^2$ (Fig. 1). This region has a continental climate with marked seasonality changes, which is characterized by a long-lasting cold, humid winter and short other seasons. Thereby, to survive the cold season, approximately half a year of coal-fired heating events (15 October to the following 15 April) occur, which emit gaseous pollutants, as well as PM, around the clock. The main industries include thermal power plants, the coal-energy-based biochemical industry, the dairy industry, the petrochemical industry, etc., which also emit atmospheric pollutants continuously. Thus, high concentrations of PM pollution dominated the major contamination cases during the winter season (data obtained from the Department of Ecology and Environment of Inner Mongolia Autonomous Region, http://sthjt.nmg.gov.cn/, last access: 16 October 2020) and gradually emerged as the limiting factor to regional ambient air quality and human health.

In this study, observations were conducted at the Inner Mongolia Environmental Monitoring Center (40°49′22″ N, 111°45′2″ E) on top of a 16-story building (∼ 40 m a.g.l. – above ground level) located in the eastern part of the downtown area near the People's Government of Inner Mongolia Autonomous Region building near the 2nd Ring Road from

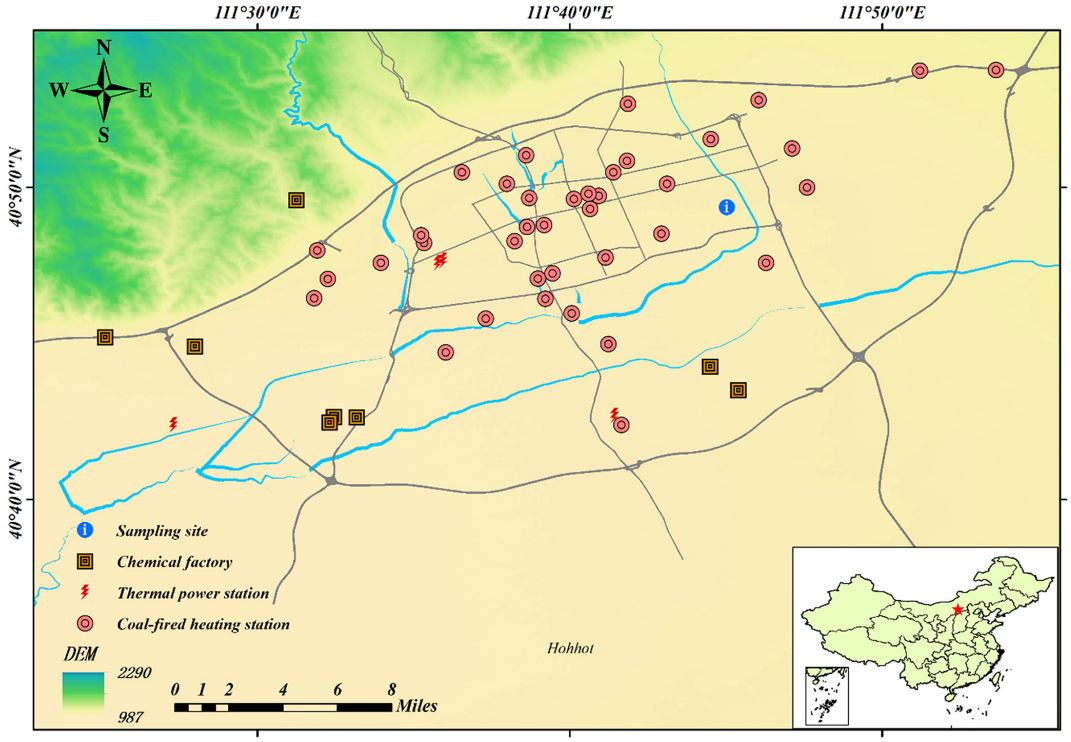

Figure 1. Map of sampling sites and coal-fired enterprises.

1 December 2019 to 31 January 2020. Residential and administrative regions were characterized by the major functional domain near the sampling site, with no direct industrial regions nearby.

2.2 Data acquisition and analysis methods

2.2.1 Data acquisition

An online ion-chromatograph instrument (MARGA ADI 2080, Metrohm Applikon, Switzerland) was employed to simultaneously determine the water-soluble inorganic ions (Na^+, NH_4^+, Mg^{2+}, Ca^{2+}, K^+, Cl^-, F^-, SO_4^{2-}, NO_3^-) in $PM_{2.5}$ and corresponding trace gases (SO_2, HNO_2, HNO_3, HCl, NH_3). This instrument has been widely used in previous work (Rumsey et al., 2014; Nie et al., 2015; Huang et al., 2020), and the details are listed in the Supplement (Sect. S1.1). Correspondingly, gaseous pollutants (e.g., NO_x, CO, PM_1, $PM_{2.5}$, PM_{10}) and meteorological datasets (e.g., wind speed, wind direction, RH, temperature), as well as the adopted models, can be found in our previous work (Xie et al., 2021). In addition, peroxyacetyl nitrates (PANs), nitrous oxide (N_2O) and solar spectrophotometry were measured by PAN 100 (Focused Photonics Inc.), N_2O monitor (LSE Monitors) and CE-318T (CIMEL), respectively.

2.2.2 Analysis methods

Generally, the sulfur oxidation ratio (SOR) and the nitrogen oxidation ratio (NOR) were calculated as follows, which were used to indicate the contribution of secondary transformation during the haze events (Song et al., 2007; Zhou et al., 2018).

$$\mathrm{SOR} = \frac{n\left(\mathrm{SO_4^{2-}}\right)}{n\left(\mathrm{SO_2}\right) + n\left(\mathrm{SO_4^{2-}}\right)} \quad (1)$$

$$\mathrm{NOR} = \frac{n\left(\mathrm{HNO_3}\right) + n\left(\mathrm{NO_3^-}\right)}{n\left(\mathrm{NO_2}\right) + n\left(\mathrm{HNO_3}\right) + n\left(\mathrm{NO_3^-}\right)} \quad (2)$$

Meanwhile, as an indicator of ammonia conversion efficiency, the ammonia transition ratio (NTR) was calculated as the following equation (all units are $\mu g\,m^{-3}$).

$$\mathrm{NTR} = \frac{\mathrm{NH_4^+}/18}{\mathrm{NH_4^+}/18 + \mathrm{NH_3}/22.4} \quad (3)$$

In addition, as the fractions of ammonia, nitrate and sulfate in deliquesced aerosol, $\varepsilon\ (\mathrm{NO_3^-})$, $\varepsilon\ (\mathrm{NH_4^+})$ and $\varepsilon\ (\mathrm{SO_4^{2-}})$ were expressed as follows.

$$\varepsilon\left(NO_3^-\right) = \frac{n\left(NO_3^-\right)}{n\left(HNO_3\right) + n\left(NO_3^-\right)} \quad (4)$$

$$\varepsilon\left(NH_4^+\right) = \frac{n\left(NH_4^+\right)}{n\left(NH_3\right) + n\left(NH_4^+\right)} \quad (5)$$

$$\varepsilon\left(SO_4^{2-}\right) = \frac{n\left(SO_4^{2-}\right)}{n\left(SO_2\right) + n\left(SO_4^{2-}\right)} \quad (6)$$

2.2.3 Aerosol pH

In this work, a widely used thermodynamic model, ISORROPIA-II (Song et al., 2018; Gao et al., 2020), was employed to establish aerosol acidity. Including the concentrations of water-soluble ions (WSIs) in $PM_{2.5}$ and gaseous pollution (e.g., NH_3, HCl), the simultaneously measured temperature and RH data were imported into its Na^+–K^+–Ca^{2+}–Mg^{2+}–NH_4^+–SO_4^{2-}–NO_3^-–Cl^-–H_2O aerosol system. According to a previous study (Song et al., 2018) and our data profiles, "forward mode" and "metastable state" were selected in the model of ISORROPIA-II to calculate aerosol acidity (H^+_{air}, H^+ loading per volume air – $\mu g\,m^{-3}$) and ALWC. Then the aerosol pH was calculated by the following equation.

$$pH = -\log_{10}\frac{1000H^+_{air}}{ALWC} \quad (7)$$

The concentrations of NH_3, NH_4^+, NO_3^- and SO_4^{2-} modeled by this model significantly correlated with their measured values with correlation coefficients of 0.971–0.999, indicating the accuracy and acceptability of the model in this work (Fig. S1 in the Supplement).

2.2.4 Heterogeneous sulfate production

Due to the necessity of precise SO_4^{2-} generation, heterogeneous sulfate production (P_{het}) was parameterized and calculated according to the following equation (Jacob, 2000; B. Zheng et al., 2015).

$$P_{het} = \frac{3600\,s\,h^{-1} \times 96\,g\,mol^{-1} \times P}{R \times T}\left(\frac{R_p}{D_g} + \frac{4}{\upsilon\gamma}\right)^{-1} S_p\left[SO_2(g)\right], \quad (8)$$

where P_{het} is presented in micrograms per cubic meter per hour ($\mu g\,m^{-3}\,h^{-1}$), $3600\,s\,h^{-1}$ is the time conversion factor, $96\,g\,mol^{-1}$ is the molar mass of SO_4^{2-}, P is atmospheric pressure (in kPa), R is the gas constant with the value of $8.31\,Pa\,m^{-3}\,mol^{-1}\,K^{-1}$, T is the temperature (in K), R_p represents the radius of aerosol particles (m), D_g is the SO_2 molecular diffusion coefficient, and υ is the mean molecular speed of SO_2 with the typical tropospheric value of $2 \times 10^{-5}\,m^2\,s^{-1}$ and $300\,m\,s^{-1}$. γ is the uptake coefficient of SO_2 on aerosols, and S_p is the aerosol surface area per unit volume of air ($m^2\,m^{-3}$) (Jacob, 2000). $PM_{2.5}$ mass concentrations ($\mu g\,m^{-3}$) and mean radius (m) during the campaign were roughly calculated utilizing the following empirical formula published by Guo et al. (2014).

$$R_p = \left(0.254 \times C_{(PM_{2.5})} + 10.259\right) \times 10^{-9} \quad (9)$$

The mean density of particles ρ was calculated as $1.5 \times 10^6\,g\,m^{-3}$ using the volume and surface area formulas of a sphere (Guo et al., 2014). S_p was estimated from the following formula.

$$S_p = \frac{C_{(PM_{2.5})} \times 10^{-6}\,g\,\mu g^{-1}}{4/3 \cdot \pi R_p^3 \cdot \rho} \cdot 4\pi R_p^2 \quad (10)$$

Relative-humidity-dependent γ values were derived according to B. Zheng et al. (2015) during the campaign in this work and are shown as the following formula.

$$\gamma = \begin{cases} 2 \times 10^{-5}, & \Psi \le 50\,\%, \\ 2 \times 10^{-5} + \frac{5\times10^{-5}-2\times10^{-5}}{100\,\%-50\,\%} \times (\Psi - 50\,\%), & 50\,\% \le \Psi \le 100\,\%, \end{cases} \quad (11)$$

where ψ refers to RH (with the unit of %).

3 Results and discussion

Based on National Ambient Air Quality Standards of China (HJ633-2012) (https://www.mee.gov.cn/ywgz/fgbz/bz/bzwb/jcffbz/201203/t20120302_224166.shtml, last access: 28 May 2020), an air quality index (AQI) was introduced in this work to classify pollution levels (Wang et al., 2015; Kanchan et al., 2015; Xu et al., 2017) and outline the characteristics of atmospheric pollutants. Briefly, daily concentrations of $PM_{2.5}$ ranging from 0–75, 75–115, 115–150, 150–250 and $> 250\,\mu g\,m^{-3}$ were classified as clean (C), lightly polluted (L), moderately polluted (M), heavily polluted (H) and seriously polluted (S) periods, respectively.

3.1 The observed evidence for the ammonia-rich atmosphere

The characteristics of atmospheric pollutants and meteorological parameters during the studied period were summarized (Sect. S2.1). In this work, molar ratios of NH_4^+ vs. anions were used to identify the chemical species of ammonium salts (Zhou et al., 2018; Wang et al., 2021; Z. Liu et al., 2017; Shi et al., 2019). The calculated results (Sect. S2.2) showed the predominant chemical species of ammonium gradually varied from the coexistence of ammonium sulfate ($(NH_4)_2SO_4$) and ammonium nitrate (NH_4NO_3) to the coexistence of $(NH_4)_2SO_4$, NH_4NO_3 and ammonium chloride (NH_4Cl) with haze aggravation (Fig. S5). Further, the

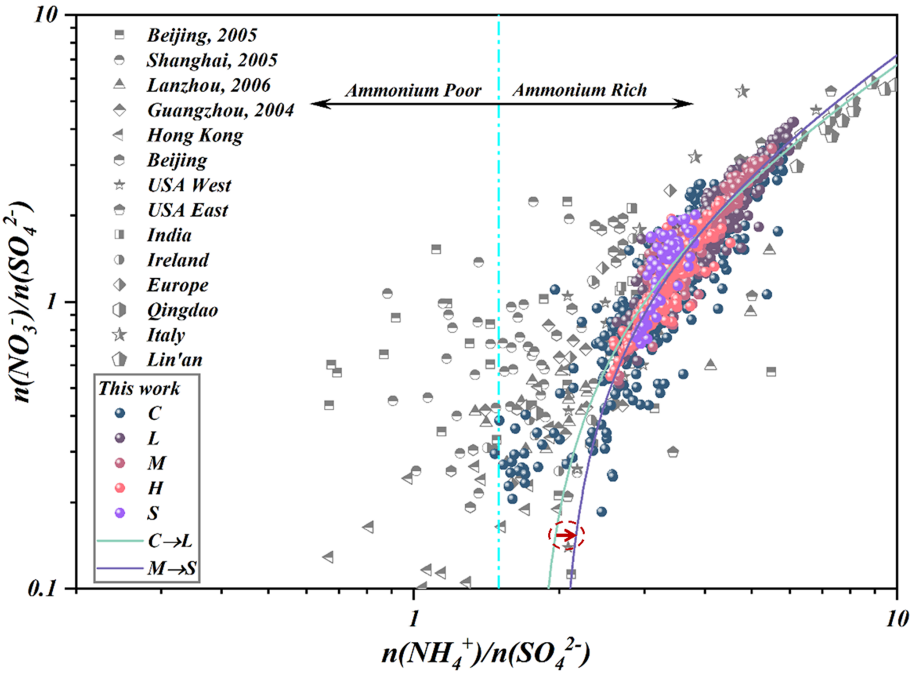

Figure 2. Nitrate to sulfate molar ratio as a function of ammonium to sulfate molar ratio.

slope of the fitted equation between excess NH_4^+ and anions was still lower than the 1 : 1 line after all the measured anions were neutralized, indicating an ammonia-rich atmosphere (Fig. S5c). Considering the national demand for ultra-low-emissions activities (nearly 2 times lower than the former national standard) for gaseous pollutants, the heavy usage of ammonia-containing compounds in the process of desulfurization and denitrification (Solera García et al., 2017; Tan et al., 2017) at widely distributed thermal power plants (> 300 000 kWh) and the close-set coal-fired heating stations (Fig. 1) resulting in ammonia fugitives provided a reasonable explanation for this ammonia-rich atmosphere. Even though retrofitting because of the national demand for ultra-low-emissions activities has been completed, distributed coal-based enterprises could also emit substantial SO_2 and NO_2 and, being subjected to heterogeneous reactions, further generate sulfate and nitrate, which aggravated the haze events (Fig. S7a and b).

To show the reaction between ammonia and nitric acid and the other formation processes of nitrate in different (relative) concentrations of sulfate, the data of previous studies and different pollution levels (C, L, M, H, S) in this work are plotted in Fig. 2. When $[NH_4^+]/[SO_4^{2-}] \leq 1.5$, the nitrate formation was associated with crustal elements rather than ammonium; when $[NH_4^+]/[SO_4^{2-}] > 1.5$, the homogeneous gas-phase reactions between NH_3 and HNO_3 became the major pathway for atmospheric ammonia to form NH_4NO_3 (Pathak et al., 2009; Liu et al., 2019). The results illustrated that the ammonia-rich regimes not only were found in Hohhot but were also observed in Guangzhou (Huang et al., 2011), Chengdu (Huang et al., 2018), Lanzhou, western and eastern USA, India, Ireland, Europe, Qingdao, Italy and Lin'an (Pathak et al., 2009) in recent decades (Fig. 2). It suggested that atmospheric oxidative modifications in the ammonia-rich atmosphere should be a widespread atmospheric issue with significant contributions to SIA generation. It is worth noting that the slopes of our data were becoming steeper, coupled with the NO_3^-/SO_4^{2-} ratio change from ∼ 4 to about 1, as the pollution levels increased. The high $PM_{2.5}$ nitrate concentration during heavy and serious stages cannot be explained by the homogeneous gas-phase reaction involving ammonia and nitric acid, which may be associated with the heterogeneous reaction of ALW on the surface of the preexisting aerosols.

3.2 Driving mechanisms of SIA formation

3.2.1 Aerosol liquid water

Our results showed that SOR, NOR and SIAs in $PM_{2.5}$ presented increasing trends with the increasing ALWC during the five pollution levels. The variation in predominant chemical species of ammonium (Fig. 2) indicated more SIAs will be generated on particles with the simultaneous increase in ALWC and $PM_{2.5}$ (Fig. 3b). Theoretically, the inorganic compound conversion was enhanced via aqueous-phase chemistry on moist particles owing to the continuous partitioning of gaseous pollutants (e.g., SO_2, NO_2, N_2O_5) in ALW and then disrupted the equilibrium between the gaseous and condensed phases, resulting in the aggravation of haze events (Xue et al., 2014; Wu et al., 2018;

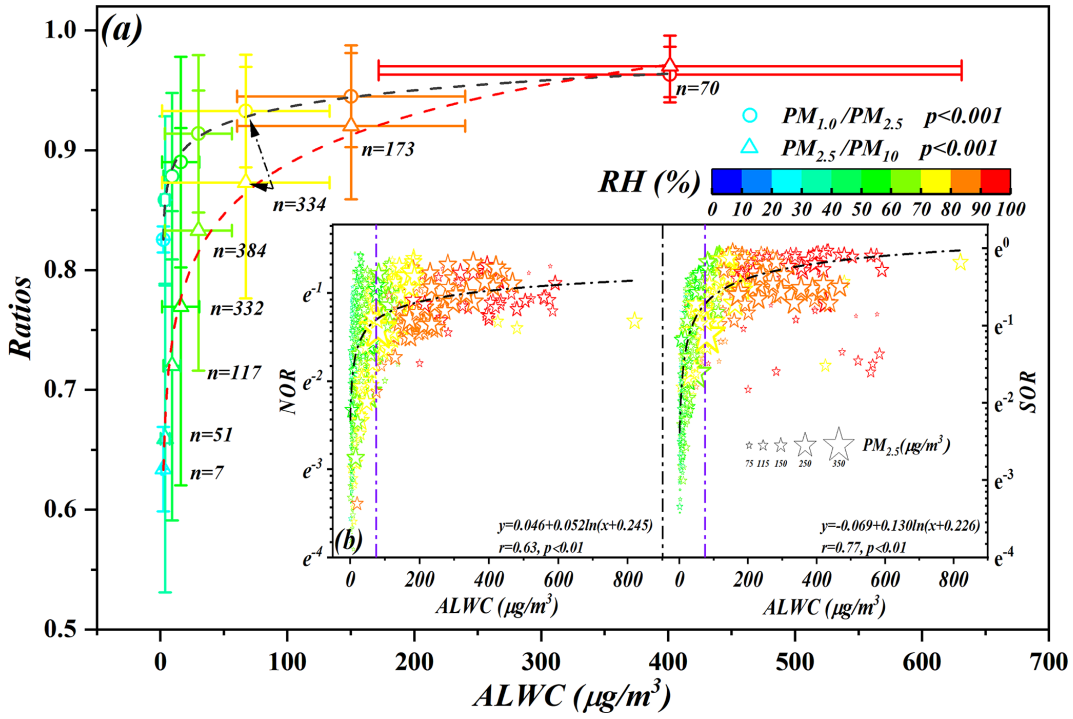

Figure 3. **(a)** Correlations between ALWC and ratios of PM response to relative humidity evolutions; **(b)** correlations between ALWC and NOR and SOR in their response to different pollution stages; the pentagrams are colored as a function of relative humidity.

G. J. Zheng et al., 2015; Wang et al., 2016). Considering seasonal heating characteristics, the shift in the equilibrium between gaseous and condensed phases was enhanced with the increasing atmospheric pollutant concentrations due to the coal-fired combustion events in winter. In detail, owing to their hygroscopic nature, the particles must increase their water contents via ALW along with RH (Fig. S8a) to maintain thermodynamic equilibrium and water vapor and simultaneously enhance the oxidation and dissolution of precursors in the micro-solution (the ALW) of the particulates. This process elevated the inorganic mass fraction, as well as particulate mass concentrations, during different pollution stages (Fig. S8b) (Bertram et al., 2009; Wang et al., 2016; B. Zheng et al., 2015; Cheng et al., 2016). Due to the larger affinity of H_2SO_4 for NH_3 (aqueous – aq), sulfate was preferentially and fully neutralized by ammonium in the ammonia-rich atmosphere to generate the non-volatile nature of $(NH_4)_2SO_4$ (Z. Liu et al., 2017; Zhou et al., 2018; Wang et al., 2021). Thus, SOR presented higher exponential growth, with the elevated ALWC coupling with more sulfate production (Fig. 3b). Concomitantly, the preferentially generated $(NH_4)_2SO_4$ further enhanced the hygroscopicity of particulate matter, in turn helping more ammonia partition into moist particulate matter and generating ammonium salts, which accelerated haze aggravation (Figs. S6 and S8c). Thus, most important of all, the sharp increase in inorganic compounds associated with the elevated ALWC significantly modified the specific surface area of particulates and further accelerated the hygroscopic aerosol growth, which simultaneously provided a substrate for the ensuing heterogenous reaction and accelerated the evolution of haze events. Previous work reported that particles of different modes made different contributions to ALWC, with the contributions of nuclear, Aitken, accumulation and coarse modes assessed at $< 1\,\%$, $3\,\%$, $85\,\%$ and $12\,\%$, respectively, indicating that the contribution of accumulation mode particles to ALWC dominated among all the aerosol particle modes (Tan et al., 2017). It indicated that secondary aerosol formation mainly happens on these fine particles, as the surface area and volume of the fine particles are much larger than those of the coarse particles. Thus, the observed significant correlations of ALWC with the ratios ($PM_{1.0}$ / $PM_{2.5}$ and $PM_{2.5}$ / PM_{10}) in this work also indicated that the hygroscopic growth of fine particulate matter ($D_p \leq 2.5\,\mu m$) is strongly associated with ALWC (Fig. 3a). Both previous work and our monitoring results suggested that the ratios of $PM_{1.0}$ / $PM_{2.5}$ and $PM_{2.5}$ / PM_{10} presented the potential possibility to index the hygroscopic growth of particulate matter.

3.2.2 Perturbation gases

Due to the strict control of SO_2, atmospheric concentrations of NO_2 and NH_3 gradually became the decisive reactive precursors for regional atmospheric secondary particulate matter generation. Thus, the state-of-the-art framework proposed by Nenes et al. (2020) was carried out to ex-

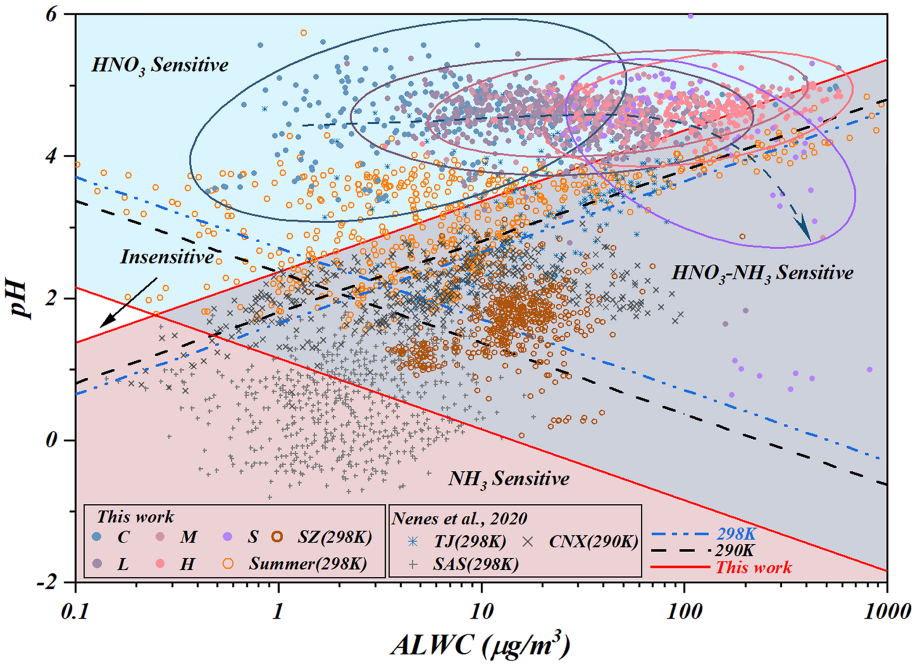

Figure 4. Chemical domains of aerosol response to ammonia and nitrate emissions.

amine the chemical domain classifications and the decisive precursor based on the datasets of previous studies (Nenes et al., 2020) and this work (Fig. 4). Due to the thermodynamically stable property of the preferentially generated $(NH_4)_2SO_4$, the semi-volatile NH_4NO_3 dominates the partitioning of ${NH_3}^T$ (sum of NH_3 and NH_4^+, same as ${NO_3}^T$) and ${NO_3}^T$. Although aqueous NO_3^- concentrations varied with haze processes, the calculated ε (${NO_3}^T$) (detailed calculated method can be found in Sect. S1.2), which was an equilibrium parameter between gaseous HNO_3 and particle-phase NO_3^- (Guo et al., 2016; Fang et al., 2017), consistently presented full loadings of nitrate on the existing particulates during the studied period (Fig. S9a and b). This could provide clear evidence for the initial HNO_3-sensitive area and continuous control of HNO_3 during the studied periods. However, with haze aggravation, significant elevated ALWC resulted in more precursors partitioning into microdroplets to maintain water vapor. This process induced a positive shift in HNO_3 dissolution equilibrium and led to more HNO_3 partitioned on particles driven by Henry's law (e.g., $HNO_{3(g)} \leftrightarrow HNO_{3(aq)}$, $K_H = 2.07\,\mathrm{mol\,(L\,Pa)^{-1}}$. Meanwhile, HNO_3 and HONO could also be produced through the reactions of $NO_2 + H_2O \xrightarrow{\text{Het}} HNO_3 + HONO$ (Huang et al., 2018). Accordingly, the OH radicals generated by HONO photolysis also contributed to these oxidation processes (Yue et al., 2020; Zhu et al., 2020). These aqueous oxidation processes were evidenced by the observation of significantly elevated HONO and PANs during the haze aggravation (Fig. S7c and d). Accordingly, the equations of $NH_4^+ + NO_3^- + H^+ + OH^- NH_4NO_3 + H_2O$ and $NH_4^+ + SO_4^{2-} + H^+ + OH^- \rightarrow (NH_4)_2SO_4 + H_2O$ were shifted to generate more NH_4NO_3 and $(NH_4)_2SO_4$ (Nenes et al., 2020; Xie et al., 2020) due to the driving force of more ammonia partitioned in elevated ALWC ($NH_3 + H_2ONH_3 \cdot H_2O$, $NH_3 \cdot H_2ONH_4^+ + OH^-$). Therefore, NH_3 and NO_x became the decisive factors for regional atmospheric oxidability in the ammonia-rich regime (Zhai et al., 2021; Tan et al., 2017; Liu et al., 2019; Li et al., 2019).

Generally, both NH_3 and HNO_3 were the limiting factors governing the generation of aerosols for cities of North China due to high loadings of atmospheric ammonia, while NH_3 governed PM formation in the southeast USA (SAS) (Zhao et al., 2020). Thanks to the raw data of Shenzhen (SZ) (Wang et al., 2022), we also calculated the ALWC and aerosol pH using ISORROPIA-II, and the scatters of SZ suggested an obvious chemical transition from a HNO_3–NH_3-sensitive regime to a NH_3-sensitive regime due to the differently originating air masses. Although both cities are located in the USA, the findings in California (CNX) were quite interesting and distributed in the insensitive region and the combined NH_3–HNO_3-sensitive region due to the moderate NH_3 levels and the complicated atmospheric conditions during the observations (Nenes et al., 2020). In our work, the data points (541/744) in summer ($pH = 3.47 \pm 1.29$) mostly laid in the HNO_3-sensitive region, while chemical domains of perturbation gas limiting the generation of secondary particulate matter presented obvious shifts from a HNO_3-sensitive to a HNO_3- and NH_3-co-sensitive regime with the haze aggravation in winter. Some data points of this work laid in the combined NH_3–HNO_3 region in winter owing to the more

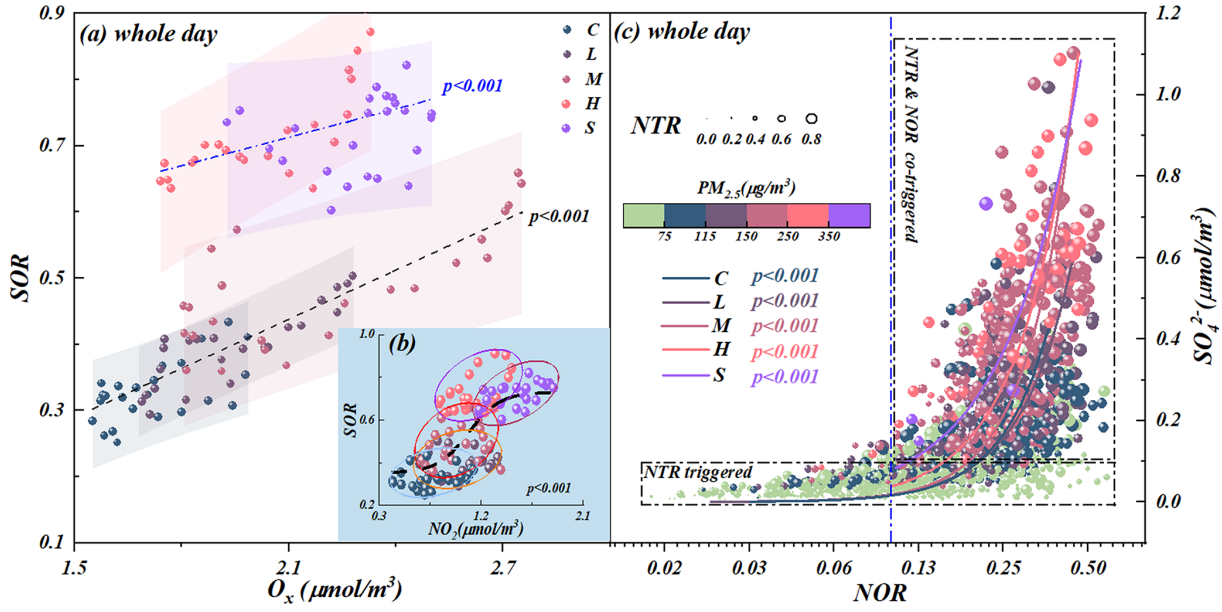

Figure 5. Correlations between **(a)** O_x and SOR, **(b)** NO_2 and SOR, and **(c)** NOR and SO_4^{2-}.

acidic conditions. Under the stable pH of aerosols in winter in Hohhot (pH = 4–5), the more important detail is that a fraction of points will distribute in the combined NH_3–HNO_3 region when ALWC > 75 μg m^{-3}, which may be attributed to the aqueous chemical transformation driven by Henry's law mentioned above due to the elevated ALWC. Comparatively, the aerosol pH in summer was significantly lower than that in winter in Hohhot. Compared to TJ (Tianjin) and SZ (Shenzhen), the aerosols pH of Hohhot in winter was also significantly higher (Fig. 4) due to the acidity of atmospheric PM being largely dependent on the alkaline material in surface soils in arid and semi-arid regions and the elevated atmospheric ammonia. In terms of seasonal characteristics, the higher temperature in summer elevates the volatility of NH_4NO_3 and dominates the partitioning of $NH_3{}^T$ in the atmospheric phase to decrease the pH of aerosols. Therefore, as can be seen from Fig. 4, the data points measured in winter in Hohhot are characterized by higher pH and lower ALWC than those in summer (Hohhot, SAS, CNX, SZ). According to the framework of Nenes et al. (2020), the transition points of Hohhot (whether winter or summer) between NH_3-dominated and HNO_3-dominated sensitivity also occur at a pH of around 2 but at lower levels of ALWC. Theoretically, it should be associated with the higher aridity of Hohhot, located in the arid and semi-arid regions of China. Our results provide the evidence for "the additional insight" proposed by Nenes et al. (2020) that the transition ALWC varies with season change and the aridity of sites in response to seasonal variability and climate change. Although this effort could provide a sound explanation for limiting gaseous pollutants in PM formation, mechanisms on their chemical domains, especially the roles of ALW in different locations under various conditions, need further study in the future.

3.2.3 The shifting of SIA formation mechanisms driven by ALW

It is worth noting that two independent correlations were found between SOR and odd oxygen (O_x, $O_x = NO_2 + O_3$) during the aggravating processes of haze events, indicating the differential mechanisms of atmospheric oxidability in sulfate generation at different stages (Fig. 5a). Different to inefficient homogeneous sulfate oxidation efficiency (Fig. S10), significant-correlation pairs of NO_2 with SOR (Fig. 5b) and NOR with SO_4^{2-} (Fig. 5c) suggested the haze aggravation was largely related to the regional NO_2 levels due to the regulating effects on atmospheric oxidability. Thus, the aqueous-phase oxidation of S(IV) by NO_2 (aq) was triggered and accelerated by the increasing ALWC and the following equation (Yao et al., 2020; Wang et al., 2016) (Fig. S11a).

$$S(IV) + NO_2(aq) + H_2O \rightarrow S(VI) + H^+ + NO_2^- \quad (R1)$$

Meanwhile, sharp logarithmic increases between SOR and NH_4^+ were also observed from the clean to moderate pollution stages (Fig. S12). Due to the joint effects of the ammonia-rich atmosphere and ammonia's extremely water-soluble property, sufficient hydroxide generated by ammonia dissolution forced the NO_2 partitioned in ALW to maintain pH through neutralization, producing sulfate via Reaction R1. Thus, the following Reaction R2 was derived by considering the processes of ammonia hydrolysis, which is evidenced by Fig. S11b.

$$S(IV) + NO_2(aq) + NH_3(aq) + H_2O \rightarrow S(VI) + NH_4^+ + NO_2^- + H^+ + NO_3^- \quad (R2)$$

Generally, NOR < 0.1 means insignificant nitrogen oxide oxidation; therefore the observed regime shift in nitrate and ammonia chemical behavior in sulfate generation suggested sulfate generation was preferentially triggered by the high ammonia utilization and then accelerated by the co-effects of ammonia utilization and nitrogen oxide oxidation (Fig. 5c).

Accordingly, Reaction R2 was activated due to the increased ALWC forcing more ammonia to partition into moist particulate matter driven by Henry's law in the ammonia-rich atmosphere ($NH_{3(g)} \rightarrow NH_{3(aq)}$) (Fig. S9c) (Clegg et al., 1998; Wu et al., 2018; Xie et al., 2020). Meanwhile, our calculated aqueous-generated NO_3^- nicely matched the theoretical aqueous-nitrate generation curve (the solid blue line in Fig. S9b) proposed by Guo et al. (2017), suggesting the pathway of fast sulfate formation from the oxidation of S(IV) by NO_2 to generate HONO (Wang et al., 2020) (Fig. S11) via Reaction R2. As a result, the thermodynamically stable $(NH_4)_2SO_4$ would be preferentially formed to maintain its water vapor pressure and thermodynamic equilibrium and then trigger the haze formation. Thus, the mentioned effects resulted in a pronounced increase in NH_3 partitioning with the haze aggravation, suggesting the importance of ammonia partitioning in sulfate generation, namely, the NTR-controlled regime with ALWC < 75 µg m^{-3}. In summary, when ALWC < 75 µg m^{-3}, the sulfate generation was preferentially triggered by high ammonia utilization and then accelerated by nitrogen oxide oxidation from clean to light pollution stages (Fig. 5c) with NOR < 0.3, SOR < 0.4 and NTR < 0.7. In this period, the chemical composition of SIAs was characterized by the moral ratio of $NO_3^- : SO_4^{2-} = 2 : 1$ (Fig. 6).

When ALWC > 75 µg m^{-3}, the haze was aggravated from moderate to serious stages along with the increasing ALWC. As a result of an increase in ALW, a large amount of H^+ was dissociated during the generation of ammonium sulfate (Fig. S13a). From light to moderate pollution stages, the solubility of SO_2 driven by Henry's law was self-limiting due to the acidity effect in low ALWC (with ALWC < 75 µg m^{-3}). Therefore, low sulfate concentrations were coupled with low ALWC at the beginning of a haze event (Fig. S13a). However, due to the co-effects of elevated ALWC and the hygroscopic nature of pre-generated ammonium sulfate, H^+ concentrations were diluted and had nearly constant in situ pH with the increase in ALWC during heavy and serious pollution stages (Fig. S14) (Wang et al., 2016; Clifton et al., 1988; Huie and Neta, 1986; Lee and Schwartz, 1983). Hence, the significantly elevated ALWC provided more chances for the partitioning of SO_2, NO_2 and NH_3 in ALW from moderate to serious pollution stages. Theoretically, Henry's constant of NO_2 (9.74×10^{-8} mol (L Pa)$^{-1}$) is 3–4 orders of magnitude lower than those of SO_2 (1.22×10^{-5} mol (L Pa)$^{-1}$) and NH_3 (6.12×10^{-4} mol (L Pa)$^{-1}$); however, it is worth noting that the aqueous-generated NO_3^- from moderate to serious stages rapidly increased 2–5 times higher than clean and light stages (Fig. S9b). Meanwhile, according to our monitoring results, the solar spectrophotometry at 380 nm during moderate to serious stages was significantly lower than that in the clean stage (Fig. S15), suggesting the aqueous oxidation of NO_2 was predominant compared to chain photolysis (Huang et al., 2018). Accordingly, it could be deduced that the aqueous-phase chemistry reaction of SO_2 and NH_3 in ALW, driven by Henry's law, became the dominant mechanism for sulfate formation due to more NO_2 being required to take part in the fast sulfate formation with the increase in ALWC in the ammonia-rich atmosphere by Reaction R2. Thus, with the increasing ALWC, high concentrations of sulfate and nitrate with high SOR (0.5–0.9), NOR (0.3–0.5) and NTR (> 0.7) induced the haze events to reach heavy and serious levels (Fig. 5c). Simultaneously, the calculated heterogeneous sulfate production rate (Jacob, 2000; McNeill, 2015) (Fig. S16) presented similar trends to the impacts of ammonia on sulfate production during different pollution stages (Xue et al., 2016; Cheng et al., 2016; Liu et al., 2020). It further stated the environmental significance of the partitioning of SO_2 and NH_3 between gas and aqueous (ALW) phases for SIA formation and haze aggravation. Our results provided the evidence of significant negative correlations between HONO and N_2O (Fig. S17) from moderate to serious stages and positive correlations between HONO and SOR (Fig. S11a), highlighting the recently reported secondary aqueous-phase oxidation pathway of SO_2 by HONO from the moderate pollution period ($2N(III) + 2S(IV) \rightarrow N_2O \uparrow + 2S(VI)$ + other products) (Wang et al., 2020). In summary, when ALWC > 75 µg m^{-3}, the aqueous-phase chemistry reaction of SO_2 and NH_3 in ALW became the prerequisite for SIA formation driven by Henry's law in the ammonia-rich atmosphere during heavy and serious stages with high SOR (0.5–0.9), NOR (0.3–0.5) and NTR (> 0.7). In this period, the chemical composition of SIAs was characterized by the moral ratio of $NO_3^- : SO_4^{2-} = 1 : 1$ (Fig. 6).

3.2.4 The positive feedback of sulfate on nitrate production

Previous works suggested that the homogeneous reaction of NO_2 with OH radicals during daylight and heterogeneous hydrolysis of N_2O_5 at night were the main routes of nitrate formation during haze episodes (He et al., 2018; Liu et al., 2019, 2020). Unsurprisingly, higher nitrate production rates (ΔNO_3^-, the difference in hour concentrations and matrixing afterwards) were frequently observed under ammonia-rich conditions due to the ammonia-rich regime being more conducive to nitrate generation. However, the high level of nitrate production rates (ΔNO_3^-) was found in the area characterized by high ammonium and low sulfate levels, suggest-

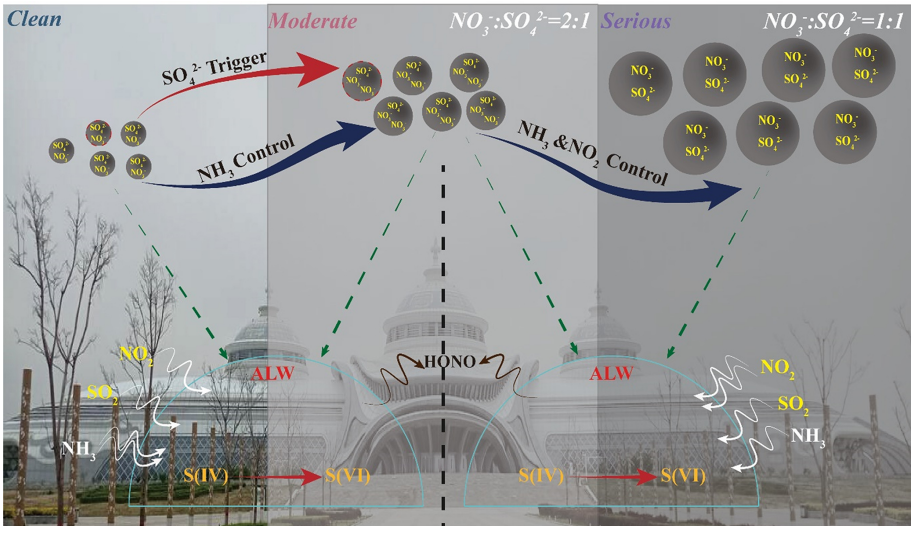

Figure 6. The characteristics and formation mechanisms of SIAs during haze aggravation.

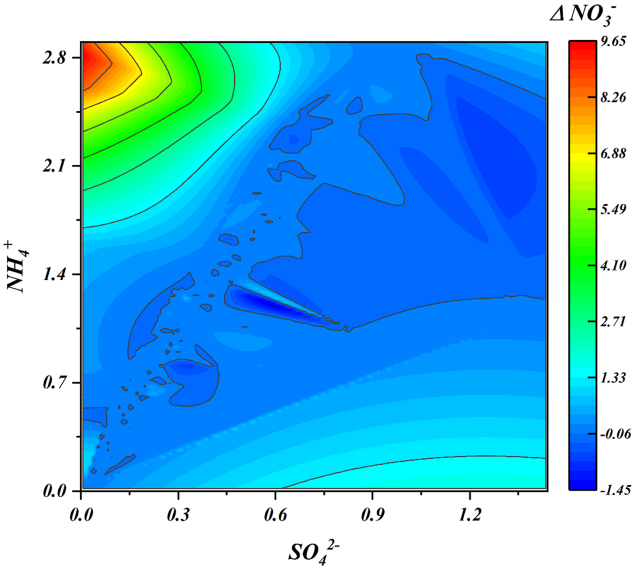

Figure 7. Direct observations of nitrate production facilitated by initially generated sulfate. (All data were matrixed to avoid interference caused by dimensionality.)

ing that utilizing ammonium and pre-generated sulfate promotes particle-phase nitrate generation (Fig. 7).

Here, we proposed a hypothesis about the hydrogen ion concentration to respond to the above observations. As is known to all, apart from the extremely low levels of crustal elements, ammonia is the only alkaline gas to neutralize the acidic gases in the atmosphere and generate ammonium ions (Xie et al., 2020). Thus, the concentrations of particulate sulfate and nitrate are affected by the partitioning of NH_4^+ and NH_3. Thereby, higher values of ΔNO_3^- and ΔSO_4^{2-} always occurred in the regions with more ammonium ions and were not confused (Figs. 7 and S18). According to both our results and published laboratory work (Wang et al., 2016), the acidity of the particulate matter could be significantly modified by the bulk aqueous reaction between NO_2 and SO_2, in which this reaction could be further enhanced due to the presence of NH_3. As a result of the increase in RH, the partitioning of atmospheric ammonia was broken to a great extent, which enhanced the neutralization of S(VI) by ammonia at the particle surface to generate ammonium sulfate and dissociate large H^+ (Fig. S13b, red part). Simultaneously, the ALWC did not rise significantly (Fig. S14b) at the beginning of haze events with relatively low sulfate concentrations. Thus, hydrogen ions generated from sulfate dissociation absorb ammonia more effectively from the ammonia-rich atmosphere at low relative humidity during the early pollution stages, which significantly promotes the net nitrate production. However, due to the co-effects of elevated RH and the hygroscopic nature of pre-generated ammonium sulfate, H^+ concentrations were diluted and shown as nearly constant in situ pH (Fig. S14a). According to previous works, the reaction between sulfate generated first and bisulfate with ammonia was treated as the determination reaction for particle acidity (Weber et al., 2016; M. Liu et al., 2017). This reaction is self-limiting due to the acidity effect, namely that it increases the acidity of the aqueous phase and in turn reduces the efficiency of Henry's constant for SO_2 solubility and reaction rate, as well as reduces the H^+ formation rates from moderate periods compared with clean periods (Fig. S13b, blue) (Wang et al., 2016; Clifton et al., 1988; Huie and Neta, 1986; Lee and Schwartz, 1983). Due to the co-effects of RH increase and the hygroscopic nature of sulfate, the ALWC was significantly elevated with the worsening of haze. Although more H^+ was generated in this process, no significant decrease in pH was found with the haze

aggravation due to the dilution effect of ALWC on H^+. Previous works suggested that, in the case of ALWC increase, nitrate production is controlled by elevated H^+ associated with the increase in sulfate; namely, NO_3^- presented an elevating trend with the increases in H^+ concentration (Xie et al., 2020). Thus, although H^+ from the dissociation of sulfuric acid and fully loaded particle nitrate in conjunction with the haze aggravation generate particle HNO_3 (Fig. S19a) could force more ammonia partitioned on the particles to generate ammonium nitrate (Fig. S19b), net nitrate production (ΔNO_3^-) was nearly consistent.

4 Conclusions

The formation of SIAs, especially sulfates and nitrates, was inherently associated with ALWC during the haze aggravation, in which the roles of ALWC should be more significant in the ammonia-rich atmosphere. The novelty of our work was finding the shifting of secondary inorganic aerosol formation mechanisms during haze aggravation and explaining the different roles of ALWC on a broader scale ($\sim 500\,\mu g\,m^{-3}$) in the ammonia-rich atmosphere based on the in situ high-resolution online monitoring datasets. The results showed that chemical domains of perturbation gas limiting the generation of secondary particulate matter presented obvious shifts from a HNO_3-sensitive to a HNO_3- and NH_3-co-sensitive regime with the haze aggravation, indicating the powerful driving effects of ammonia in the ammonia-rich atmosphere. When ALWC $< 75\,\mu g\,m^{-3}$, the sulfate generation was preferentially triggered by the high ammonia utilization and then accelerated by nitrogen oxide oxidation from clean to moderate pollution stages, characterized by NOR < 0.3, SOR < 0.4, NTR < 0.7 and the moral ratio of $NO_3^- : SO_4^{2-} = 2 : 1$. When ALWC $> 75\,\mu g\,m^{-3}$, the aqueous-phase chemistry reaction of SO_2 and NH_3 in ALW became the prerequisite for SIA formation driven by Henry's law in the ammonia-rich atmosphere during heavy and serious stages, characterized by high SOR (0.5–0.9), NOR (0.3–0.5) and NTR (> 0.7), as well as the high moral ratio of $NO_3^- : SO_4^{2-} = 1 : 1$. A positive feedback of sulfate on nitrate production was also observed in this work. Our work provides a potential explanation for the interactive mechanisms and feedback between nitric aqueous chemistry and sulfate formation in the ammonia-rich atmosphere based on high-resolution field observations. It implies the targeted controlling of haze should not simply focus on SO_2 and NO_2, but more attention should be paid to gaseous precursors (e.g., SO_2, NO_2, NH_3) and aerosol chemical constitution during different haze stages.

Data availability. All data of this study are available from the corresponding author upon reasonable request (lcw2008@imu.edu.cn).

Supplement. The supplement related to this article is available online at: https://doi.org/10.5194/acp-23-2365-2023-supplement.

Author contributions. FX: data curation, formal analysis, software, writing – original draft. YS: investigation, formal analysis. YLT: methodology, software. YSH: investigation, formal analysis. XJZ: investigation, formal analysis, software. PW: methodology, investigation. RHY: software, writing – review and editing. WW: investigation, validation, writing – review and editing. JH: investigation, methodology. JYX: investigation, validation, supervision, writing – review and editing. CWL: initiating and leading this research, supervision, writing – review and editing.

Competing interests. The contact author has declared that none of the authors has any competing interests.

Disclaimer. Publisher's note: Copernicus Publications remains neutral with regard to jurisdictional claims in published maps and institutional affiliations.

Financial support. This work is supported by the Science and Technology Major Project on Air Pollution Prevention and Prediction in Hohhot–Baotou–Ordos Cities Group of Inner Mongolia (grant no. 2020ZD0013), the National Natural Science Foundation of China (grant nos. 42167028 and 41763014), and the Science Fund for Distinguished Young Scholars of Inner Mongolia (grant no. 2019JQ05).

Review statement. This paper was edited by Zhibin Wang and reviewed by three anonymous referees.

References

Ansari, A. S. and Pandis, S. N.: Water Absorption by Secondary Organic Aerosol and Its Effect on Inorganic Aerosol Behavior, Environ. Sci. Technol., 34, 71–77, https://doi.org/10.1021/es990717q, 2000.

Bertram, T. H., Thornton, J. A., Riedel, T. P., Middlebrook, A. M., Bahreini, R., Bates, T. S., Quinn, P. K., and Coffman, D. J.: Direct observations of N_2O_5 reactivity on ambient aerosol particles, Geophys. Res. Lett., 36, L19803, https://doi.org/10.1029/2009GL040248, 2009.

Bian, Y. X., Zhao, C. S., Ma, N., Chen, J., and Xu, W. Y.: A study of aerosol liquid water content based on hygroscopicity measurements at high relative humidity in the North China Plain, Atmos. Chem. Phys., 14, 6417–6426, https://doi.org/10.5194/acp-14-6417-2014, 2014.

Carlton, A. G. and Turpin, B. J.: Particle partitioning potential of organic compounds is highest in the Eastern US and driven by anthropogenic water, Atmos. Chem. Phys., 13, 10203–10214, https://doi.org/10.5194/acp-13-10203-2013, 2013.

Cheng, Y., Zheng, G., Wei, C., Mu, Q., Zheng, B., Wang, Z., Gao, M., Zhang, Q., He, K., Carmichael, G., Pöschl, U., and Su,

H.: Reactive nitrogen chemistry in aerosol water as a source of sulfate during haze events in China, Sci. Adv., 2, e1601530, https://doi.org/10.1126/sciadv.1601530, 2016.

Clegg, S. L., Brimblecombe, P., and Wexler, A. S.: Thermodynamic Model of the System H^+–NH_4^+–SO_4^{2-}–NO_3–H_2O at Tropospheric Temperatures, J. Phys. Chem. A, 102, 2137–2154, https://doi.org/10.1021/jp973042r, 1998.

Clifton, C. L., Altstein, N., and Huie, R. E.: Rate constant for the reaction of nitrogen dioxide with sulfur(IV) over the pH range 5.3–13, Environ. Sci. Technol., 22, 586–589, https://doi.org/10.1021/es00170a018, 1988.

Davies, J. F. and Wilson, K. R.: Nanoscale interfacial gradients formed by the reactive uptake of OH radicals onto viscous aerosol surfaces, Chem. Sci., 6, 7020–7027, https://doi.org/10.1039/C5SC02326B, 2015.

Fang, T., Guo, H., Zeng, L., Verma, V., Nenes, A., and Weber, R. J.: Highly Acidic Ambient Particles, Soluble Metals, and Oxidative Potential: A Link between Sulfate and Aerosol Toxicity, Environ. Sci. Technol., 51, 2611–2620, https://doi.org/10.1021/acs.est.6b06151, 2017.

Fu, H. and Chen, J.: Formation, features and controlling strategies of severe haze-fog pollutions in China, Sci. Total Environ., 578, 121–138, https://doi.org/10.1016/j.scitotenv.2016.10.201, 2017.

Gao, J., Wei, Y., Shi, G., Yu, H., Zhang, Z., Song, S., Wang, W., Liang, D., and Feng, Y.: Roles of RH, aerosol pH and sources in concentrations of secondary inorganic aerosols, during different pollution periods, Atmos. Environ., 241, 117770, https://doi.org/10.1016/j.atmosenv.2020.117770, 2020.

Ge, B., Xu, X., Ma, Z., Pan, X., Wang, Z., Lin, W., Ouyang, B., Xu, D., Lee, J., Zheng, M., Ji, D., Sun, Y., Dong, H., Squires, F. A., Fu, P., and Wang, Z.: Role of Ammonia on the Feedback Between AWC and Inorganic Aerosol Formation During Heavy Pollution in the North China Plain, Earth Space Sci., 6, 1675–1693, https://doi.org/10.1029/2019EA000799, 2019.

Guo, H., Sullivan, A. P., Campuzano-Jost, P., Schroder, J. C., Lopez-Hilfiker, F. D., Dibb, J. E., Jimenez, J. L., Thornton, J. A., Brown, S. S., Nenes, A., and Weber, R. J.: Fine particle pH and the partitioning of nitric acid during winter in the northeastern United States, J. Geophys. Res.-Atmos., 121, 10355–10376, https://doi.org/10.1002/2016JD025311, 2016.

Guo, H., Liu, J., Froyd, K. D., Roberts, J. M., Veres, P. R., Hayes, P. L., Jimenez, J. L., Nenes, A., and Weber, R. J.: Fine particle pH and gas–particle phase partitioning of inorganic species in Pasadena, California, during the 2010 CalNex campaign, Atmos. Chem. Phys., 17, 5703–5719, https://doi.org/10.5194/acp-17-5703-2017, 2017.

Guo, S., Hu, M., Zamora, M. L., Peng, J., Shang, D., Zheng, J., Du, Z., Wu, Z., Shao, M., Zeng, L., Molina, M. J., and Zhang, R.: Elucidating severe urban haze formation in China, P. Natl. Acad. Sci. USA, 111, 17373–17378, https://doi.org/10.1073/pnas.1419604111, 2014.

Gwynn, R. C., Burnett, R. T., and Thurston, G. D.: A time-series analysis of acidic particulate matter and daily mortality and morbidity in the Buffalo, New York, region, Environ. Health Perspect., 108, 125–133, https://doi.org/10.1289/ehp.00108125, 2000.

He, P., Xie, Z., Chi, X., Yu, X., Fan, S., Kang, H., Liu, C., and Zhan, H.: Atmospheric $\Delta^{17}O(NO_3^-)$ reveals nocturnal chemistry dominates nitrate production in Beijing haze, Atmos. Chem. Phys., 18, 14465–14476, https://doi.org/10.5194/acp-18-14465-2018, 2018.

Hodas, N., Sullivan, A. P., Skog, K., Keutsch, F. N., Collett, J. L., Decesari, S., Facchini, M. C., Carlton, A. G., Laaksonen, A., and Turpin, B. J.: Aerosol Liquid Water Driven by Anthropogenic Nitrate: Implications for Lifetimes of Water-Soluble Organic Gases and Potential for Secondary Organic Aerosol Formation, Environ. Sci. Technol., 48, 11127–11136, https://doi.org/10.1021/es5025096, 2014.

Huang, R.-J., Zhang, Y., Bozzetti, C., Ho, K.-F., Cao, J.-J., Han, Y., Daellenbach, K. R., Slowik, J. G., Platt, S. M., Canonaco, F., Zotter, P., Wolf, R., Pieber, S. M., Bruns, E. A., Crippa, M., Ciarelli, G., Piazzalunga, A., Schwikowski, M., Abbaszade, G., Schnelle-Kreis, J., Zimmermann, R., An, Z., Szidat, S., Baltensperger, U., Haddad, I. E., and Prévôt, A. S. H.: High secondary aerosol contribution to particulate pollution during haze events in China, Nature, 514, 218–222, https://doi.org/10.1038/nature13774, 2014.

Huang, R.-J., Duan, J., Li, Y., Chen, Q., Chen, Y., Tang, M., Yang, L., Ni, H., Lin, C., Xu, W., Liu, Y., Chen, C., Yan, Z., Ovadnevaite, J., Ceburnis, D., Dusek, U., Cao, J., Hoffmann, T., and O'Dowd, C. D.: Effects of NH_3 and alkaline metals on the formation of particulate sulfate and nitrate in wintertime Beijing, Sci. Total Environ., 717, 137190, https://doi.org/10.1016/j.scitotenv.2020.137190, 2020.

Huang, X., Qiu, R., Chan, C. K., and Ravi Kant, P.: Evidence of high $PM_{2.5}$ strong acidity in ammonia-rich atmosphere of Guangzhou, China: Transition in pathways of ambient ammonia to form aerosol ammonium at $[NH_4^+]/[SO_4^{2-}] = 1.5$, Atmos. Res., 99, 488–495, https://doi.org/10.1016/j.atmosres.2010.11.021, 2011.

Huang, X., Zhang, J., Luo, B., Wang, L., Tang, G., Liu, Z., Song, H., Zhang, W., Yuan, L., and Wang, Y.: Water-soluble ions in $PM_{2.5}$ during spring haze and dust periods in Chengdu, China: Variations, nitrate formation and potential source areas, Environ. Pollut., 243, 1740–1749, https://doi.org/10.1016/j.envpol.2018.09.126, 2018.

Huie, R. E. and Neta, P.: Kinetics of one-electron transfer reactions involving chlorine dioxide and nitrogen dioxide, J. Phys. Chem., 90, 1193–1198, https://doi.org/10.1021/j100278a046, 1986.

Jacob, D. J.: Heterogeneous chemistry and tropospheric ozone, Atmos. Environ., 34, 2131–2159, https://doi.org/10.1016/S1352-2310(99)00462-8, 2000.

Jin, X., Wang, Y., Li, Z., Zhang, F., Xu, W., Sun, Y., Fan, X., Chen, G., Wu, H., Ren, J., Wang, Q., and Cribb, M.: Significant contribution of organics to aerosol liquid water content in winter in Beijing, China, Atmos. Chem. Phys., 20, 901–914, https://doi.org/10.5194/acp-20-901-2020, 2020.

Kanchan, K., Gorai, A. K., and Goyal, P.: A review on air quality indexing system, Asian J. Atmos. Environ., 9, 101–113, 2015.

Lavigne, E., Yasseen, A. S., Stieb, D. M., Hystad, P., van Donkelaar, A., Martin, R. V., Brook, J. R., Crouse, D. L., Burnett, R. T., Chen, H., Weichenthal, S., Johnson, M., Villeneuve, P. J., and Walker, M.: Ambient air pollution and adverse birth outcomes: Differences by maternal comorbidities, Environ. Res., 148, 457–466, https://doi.org/10.1016/j.envres.2016.04.026, 2016.

Lee, Y. N. and Schwartz, S. E.: Kinetics of Oxidation of Aqueous Sulfur(IV) by Nitrogen Dioxide, in: Precipitation Scavenging, Dry Deposition, and Resuspension, Vol. 1: Precipitation Scavenging, edited by: Pruppacher, H. R., Semonin, R. G., and Slinn,

W. G., Elsevier, New York, USA, Amsterdam, the Netherlands, Oxford, UK, 453–470, 1983.

Li, H., Cheng, J., Zhang, Q., Zheng, B., Zhang, Y., Zheng, G., and He, K.: Rapid transition in winter aerosol composition in Beijing from 2014 to 2017: response to clean air actions, Atmos. Chem. Phys., 19, 11485–11499, https://doi.org/10.5194/acp-19-11485-2019, 2019.

Liu, M., Song, Y., Zhou, T., Xu, Z., Yan, C., Zheng, M., Wu, Z., Hu, M., Wu, Y., and Zhu, T.: Fine particle pH during severe haze episodes in northern China, Geophys. Res. Lett., 44, 5213–5221, https://doi.org/10.1002/2017GL073210, 2017.

Liu, M., Huang, X., Song, Y., Tang, J., Cao, J., Zhang, X., Zhang, Q., Wang, S., Xu, T., Kang, L., Cai, X., Zhang, H., Yang, F., Wang, H., Yu, J. Z., Lau, A. K. H., He, L., Huang, X., Duan, L., Ding, A., Xue, L., Gao, J., Liu, B., and Zhu, T.: Ammonia emission control in China would mitigate haze pollution and nitrogen deposition, but worsen acid rain, P. Natl. Acad. Sci. USA, 116, 7760–7765, https://doi.org/10.1073/pnas.1814880116, 2019.

Liu, P., Ye, C., Xue, C., Zhang, C., Mu, Y., and Sun, X.: Formation mechanisms of atmospheric nitrate and sulfate during the winter haze pollution periods in Beijing: gas-phase, heterogeneous and aqueous-phase chemistry, Atmos. Chem. Phys., 20, 4153–4165, https://doi.org/10.5194/acp-20-4153-2020, 2020.

Liu, T., Chan, A. W. H., and Abbatt, J. P. D.: Multiphase Oxidation of Sulfur Dioxide in Aerosol Particles: Implications for Sulfate Formation in Polluted Environments, Environ. Sci. Technol., 55, 4227–4242, https://doi.org/10.1021/acs.est.0c06496, 2021.

Liu, Z., Xie, Y., Hu, B., Wen, T., Xin, J., Li, X., and Wang, Y.: Size-resolved aerosol water-soluble ions during the summer and winter seasons in Beijing: Formation mechanisms of secondary inorganic aerosols, Chemosphere, 183, 119–131, https://doi.org/10.1016/j.chemosphere.2017.05.095, 2017.

McNeill, V. F.: Aqueous Organic Chemistry in the Atmosphere: Sources and Chemical Processing of Organic Aerosols, Environ. Sci. Technol., 49, 1237–1244, https://doi.org/10.1021/es5043707, 2015.

Nenes, A., Pandis, S. N., Weber, R. J., and Russell, A.: Aerosol pH and liquid water content determine when particulate matter is sensitive to ammonia and nitrate availability, Atmos. Chem. Phys., 20, 3249–3258, https://doi.org/10.5194/acp-20-3249-2020, 2020.

Nguyen, T. K. V., Petters, M. D., Suda, S. R., Guo, H., Weber, R. J., and Carlton, A. G.: Trends in particle-phase liquid water during the Southern Oxidant and Aerosol Study, Atmos. Chem. Phys., 14, 10911–10930, https://doi.org/10.5194/acp-14-10911-2014, 2014.

Nie, W., Ding, A. J., Xie, Y. N., Xu, Z., Mao, H., Kerminen, V. M., Zheng, L. F., Qi, X. M., Huang, X., Yang, X. Q., Sun, J. N., Herrmann, E., Petäjä, T., Kulmala, M., and Fu, C. B.: Influence of biomass burning plumes on HONO chemistry in eastern China, Atmos. Chem. Phys., 15, 1147–1159, https://doi.org/10.5194/acp-15-1147-2015, 2015.

Nozière, B., Dziedzic, P., and Córdova, A.: Inorganic ammonium salts and carbonate salts are efficient catalysts for aldol condensation in atmospheric aerosols, Phys. Chem. Chem. Phys., 12, 3864–3872, https://doi.org/10.1039/B924443C, 2010.

Pathak, R. K., Wu, W. S., and Wang, T.: Summertime $PM_{2.5}$ ionic species in four major cities of China: nitrate formation in an ammonia-deficient atmosphere, Atmos. Chem. Phys., 9, 1711–1722, https://doi.org/10.5194/acp-9-1711-2009, 2009.

Rumsey, I. C., Cowen, K. A., Walker, J. T., Kelly, T. J., Hanft, E. A., Mishoe, K., Rogers, C., Proost, R., Beachley, G. M., Lear, G., Frelink, T., and Otjes, R. P.: An assessment of the performance of the Monitor for AeRosols and GAses in ambient air (MARGA): a semi-continuous method for soluble compounds, Atmos. Chem. Phys., 14, 5639–5658, https://doi.org/10.5194/acp-14-5639-2014, 2014.

Shang, D., Peng, J., Guo, S., Wu, Z., and Hu, M.: Secondary aerosol formation in winter haze over the Beijing-Tianjin-Hebei Region, China, Front Environ. Sci. Eng., 15, 34–46, https://doi.org/10.1007/s11783-020-1326-x, 2020.

Shi, G., Xu, J., Shi, X., Liu, B., Bi, X., Xiao, Z., Chen, K., Wen, J., Dong, S., Tian, Y., Feng, Y., Yu, H., Song, S., Zhao, Q., Gao, J., and Russell, A. G.: Aerosol pH Dynamics During Haze Periods in an Urban Environment in China: Use of Detailed, Hourly, Speciated Observations to Study the Role of Ammonia Availability and Secondary Aerosol Formation and Urban Environment, J. Geophys. Res.-Atmos., 124, 9730–9742, https://doi.org/10.1029/2018JD029976, 2019.

Shiraiwa, M., Pfrang, C., Koop, T., and Pöschl, U.: Kinetic multi-layer model of gas-particle interactions in aerosols and clouds (KM-GAP): linking condensation, evaporation and chemical reactions of organics, oxidants and water, Atmos. Chem. Phys., 12, 2777–2794, https://doi.org/10.5194/acp-12-2777-2012, 2012.

Solera García, M. A., Timmis, R. J., Van Dijk, N., Whyatt, J. D., Leith, I. D., Leeson, S. R., Braban, C. F., Sheppard, L. J., Sutton, M. A., and Tang, Y. S.: Directional passive ambient air monitoring of ammonia for fugitive source attribution; a field trial with wind tunnel characteristics, Atmos. Environ., 167, 576–585, https://doi.org/10.1016/j.atmosenv.2017.07.043, 2017.

Song, C. H., Kim, C. M., Lee, Y. J., Carmichael, G. R., Lee, B. K., and Lee, D. S.: An evaluation of reaction probabilities of sulfate and nitrate precursors onto East Asian dust particles, J. Geophys. Res.-Atmos., 112, D18206, https://doi.org/10.1029/2006JD008092, 2007.

Song, S., Gao, M., Xu, W., Shao, J., Shi, G., Wang, S., Wang, Y., Sun, Y., and McElroy, M. B.: Fine-particle pH for Beijing winter haze as inferred from different thermodynamic equilibrium models, Atmos. Chem. Phys., 18, 7423–7438, https://doi.org/10.5194/acp-18-7423-2018, 2018.

Tan, H., Cai, M., Fan, Q., Liu, L., Li, F., Chan, P., Deng, X., and Wu, D.: An analysis of aerosol liquid water content and related impact factors in Pearl River Delta, Sci. Total Environ., 579, 1822–1830, 2017.

Wang, G., Zhang, R., Gomez, M. E., Yang, L., Zamora, M. L., Hu, M., Lin, Y., Peng, J., Guo, S., and Meng, J.: Persistent sulfate formation from London Fog to Chinese haze, P. Natl. Acad. Sci. USA, 113, 13630–13635, 2016.

Wang, G., Chen, J., Xu, J., Yun, L., Zhang, M., Li, H., Qin, X., Deng, C., Zheng, H., Gui, H., Liu, J., and Huang, K.: Atmospheric Processing at the Sea-Land Interface Over the South China Sea: Secondary Aerosol Formation, Aerosol Acidity, and Role of Sea Salts, J. Geophys. Res.-Atmos., 127, e2021JD036255, https://doi.org/10.1029/2021JD036255, 2022.

Wang, H., Wang, X., Zhou, H., Ma, H., Xie, F., Zhou, X., Fan, Q., Lü, C., and He, J.: Stoichiometric characteristics

and economic implications of water-soluble ions in $PM_{2.5}$ from a resource-dependent city, Environ. Res., 193, 110522, https://doi.org/10.1016/j.envres.2020.110522, 2021.

Wang, J., Li, J., Ye, J., Zhao, J., and Jacob, D. J.: Fast sulfate formation from oxidation of SO_2 by NO_2 and HONO observed in Beijing haze, Nat. Commun., 11, 2844, https://doi.org/10.1038/s41467-020-16683-x, 2020.

Wang, S., Nan, J., Shi, C., Fu, Q., Gao, S., Wang, D., Cui, H., Saiz-Lopez, A., and Zhou, B.: Atmospheric ammonia and its impacts on regional air quality over the megacity of Shanghai, China, Sci. Rep., 5, 15842, https://doi.org/10.1038/srep15842, 2015.

Weber, R. J., Guo, H., Russell, A. G., and Nenes, A.: High aerosol acidity despite declining atmospheric sulfate concentrations over the past 15 years, Nat. Geosci., 9, 282–285, https://doi.org/10.1038/ngeo2665, 2016.

Wong, J. P. S., Lee, A. K. Y., and Abbatt, J. P. D.: Impacts of Sulfate Seed Acidity and Water Content on Isoprene Secondary Organic Aerosol Formation, Environ. Sci. Technol., 49, 13215–13221, https://doi.org/10.1021/acs.est.5b02686, 2015.

Wu, Z., Wang, Y., Tan, T., Zhu, Y., Li, M., Shang, D., Wang, H., Lu, K., Guo, S., Zeng, L., and Zhang, Y.: Aerosol Liquid Water Driven by Anthropogenic Inorganic Salts: Implying Its Key Role in Haze Formation over the North China Plain, Environ. Sci. Technol. Lett., 5, 160–166, https://doi.org/10.1021/acs.estlett.8b00021, 2018.

Xie, F., Zhou, X., Wang, H., Gao, J., Hao, F., He, J., and Lü, C.: Heating events drive the seasonal patterns of volatile organic compounds in a typical semi-arid city, Sci. Total Environ., 788, 147781, https://doi.org/10.1016/j.scitotenv.2021.147781, 2021.

Xie, Y., Wang, G., Wang, X., Chen, J., Chen, Y., Tang, G., Wang, L., Ge, S., Xue, G., Wang, Y., and Gao, J.: Nitrate-dominated $PM_{2.5}$ and elevation of particle pH observed in urban Beijing during the winter of 2017, Atmos. Chem. Phys., 20, 5019–5033, https://doi.org/10.5194/acp-20-5019-2020, 2020.

Xu, L., Duan, F., He, K., Ma, Y., Zhu, L., Zheng, Y., Huang, T., Kimoto, T., Ma, T., Li, H., Ye, S., Yang, S., Sun, Z., and Xu, B.: Characteristics of the secondary water-soluble ions in a typical autumn haze in Beijing, Environ. Pollut., 227, 296–305, https://doi.org/10.1016/j.envpol.2017.04.076, 2017.

Xue, J., Griffith, S. M., Yu, X., Lau, A. K. H., and Yu, J. Z.: Effect of nitrate and sulfate relative abundance in $PM_{2.5}$ on liquid water content explored through half-hourly observations of inorganic soluble aerosols at a polluted receptor site, Atmos. Environ., 99, 24–31, https://doi.org/10.1016/j.atmosenv.2014.09.049, 2014.

Xue, J., Yuan, Z., Griffith, S. M., Yu, X., Lau, A. K. H., and Yu, J. Z.: Sulfate Formation Enhanced by a Cocktail of High NO_x, SO_2, Particulate Matter, and Droplet pH during Haze-Fog Events in Megacities in China: An Observation-Based Modeling Investigation, Environ. Sci. Technol., 50, 7325–7334, https://doi.org/10.1021/acs.est.6b00768, 2016.

Yao, L., Fan, X., Yan, C., Kurtén, T., Daellenbach, K. R., Li, C., Wang, Y., Guo, Y., Dada, L., Rissanen, M. P., Cai, J., Tham, Y. J., Zha, Q., Zhang, S., Du, W., Yu, M., Zheng, F., Zhou, Y., Kontkanen, J., Chan, T., Shen, J., Kujansuu, J. T., Kangasluoma, J., Jiang, J., Wang, L., Worsnop, D. R., Petäjä, T., Kerminen, V.-M., Liu, Y., Chu, B., He, H., Kulmala, M., and Bianchi, F.: Unprecedented Ambient Sulfur Trioxide (SO_3) Detection: Possible Formation Mechanism and Atmospheric Implications, Environ. Sci. Technol. Lett., 7, 809–818, https://doi.org/10.1021/acs.estlett.0c00615, 2020.

Yue, F., He, P., Chi, X., Wang, L., Yu, X., Zhang, P., and Xie, Z.: Characteristics and major influencing factors of sulfate production via heterogeneous transition-metal-catalyzed oxidation during haze evolution in China, Atmos. Pollut. Res., 11, 1351–1358, https://doi.org/10.1016/j.apr.2020.05.014, 2020.

Zhai, S., Jacob, D. J., Wang, X., Liu, Z., Wen, T., Shah, V., Li, K., Moch, J. M., Bates, K. H., Song, S., Shen, L., Zhang, Y., Luo, G., Yu, F., Sun, Y., Wang, L., Qi, M., Tao, J., Gui, K., Xu, H., Zhang, Q., Zhao, T., Wang, Y., Lee, H. C., Choi, H., and Liao, H.: Control of particulate nitrate air pollution in China, Nat. Geosci., 14, 389–395, https://doi.org/10.1038/s41561-021-00726-z, 2021.

Zhang, R., Wang, G., Guo, S., Zamora, M. L., Ying, Q., Lin, Y., Wang, W., Hu, M., and Wang, Y.: Formation of Urban Fine Particulate Matter, Chem. Rev., 115, 3803–3855, https://doi.org/10.1021/acs.chemrev.5b00067, 2015.

Zhao, Q., Nenes, A., Yu, H., Song, S., Xiao, Z., Chen, K., Shi, G., Feng, Y., and Russell, A. G.: Using High-Temporal-Resolution Ambient Data to Investigate Gas-Particle Partitioning of Ammonium over Different Seasons, Environ. Sci. Technol., 54, 9834–9843, https://doi.org/10.1021/acs.est.9b07302, 2020.

Zheng, B., Zhang, Q., Zhang, Y., He, K. B., Wang, K., Zheng, G. J., Duan, F. K., Ma, Y. L., and Kimoto, T.: Heterogeneous chemistry: a mechanism missing in current models to explain secondary inorganic aerosol formation during the January 2013 haze episode in North China, Atmos. Chem. Phys., 15, 2031–2049, https://doi.org/10.5194/acp-15-2031-2015, 2015.

Zheng, G. J., Duan, F. K., Su, H., Ma, Y. L., Cheng, Y., Zheng, B., Zhang, Q., Huang, T., Kimoto, T., Chang, D., Pöschl, U., Cheng, Y. F., and He, K. B.: Exploring the severe winter haze in Beijing: the impact of synoptic weather, regional transport and heterogeneous reactions, Atmos. Chem. Phys., 15, 2969–2983, https://doi.org/10.5194/acp-15-2969-2015, 2015.

Zhou, H., Lü, C., He, J., Gao, M., Zhao, B., Ren, L., Zhang, L., Fan, Q., Liu, T., He, Z., Dudagula, Zhou, B., Liu, H., and Zhang, Y.: Stoichiometry of water-soluble ions in $PM_{2.5}$: Application in source apportionment for a typical industrial city in semi-arid region, Northwest China, Atmos. Res., 204, 149–160, https://doi.org/10.1016/j.atmosres.2018.01.017, 2018.

Zhu, Y., Li, W., Lin, Q., Yuan, Q., Liu, L., Zhang, J., Zhang, Y., Shao, L., Niu, H., Yang, S., and Shi, Z.: Iron solubility in fine particles associated with secondary acidic aerosols in east China, Environ. Pollut., 264, 114769, https://doi.org/10.1016/j.envpol.2020.114769, 2020.